ELSEVIER

Earth and Planetary Science Letters 198 (2002) 93–112

EPSL

www.elsevier.com/locate/epsl

Diffusive fractionation of trace elements during production and transport of melt in Earth's upper mantle

James A. Van Orman [a,*], Timothy L. Grove [a], Nobumichi Shimizu [b]

[a] *Department of Earth, Atmospheric, and Planetary Sciences, Massachusetts Institute of Technology, Cambridge, MA 02139, USA*
[b] *Department of Geology and Geophysics, Woods Hole Oceanographic Institution, Woods Hole, MA 02543, USA*

Received 7 January 2002; accepted 23 January 2002

Abstract

We have developed a numerical model to investigate the importance of diffusive chemical fractionation during production and transport of melt in Earth's upper mantle. The model incorporates new experimental data on the diffusion rates of rare earth elements (REE) in high-Ca pyroxene [Van Orman et al., Contrib. Mineral. Petrol. 141 (2001) 687–703] and pyrope garnet [Van Orman et al., Contrib. Mineral. Petrol., in press], including the dependence of diffusivity on temperature, pressure and ionic radius. We find that diffusion exerts an important control on REE fractionation under conditions typical of melting beneath slow spreading centers, provided that grain radii are $\sim$0.5 mm or greater. When partitioning is diffusion-limited, REE are fractionated less efficiently than under equilibrium conditions, and this effect becomes more pronounced as the melting rate, grain size, and efficiency of melt segregation increase. Data for the light REE in abyssal peridotite clinopyroxene (cpx) grains from the slow spreading America–Antarctic and Southwest Indian ridge systems are better explained by melting models that allow for diffusive exchange than by models that assume complete solid–melt equilibration. The data are best fit by models in which the initial cpx grain radii are $\sim$2–3 mm and melt extraction is very efficient (near fractional). Diffusion is likely to play a strong role in REE fractionation during intergranular melt transport in the upper mantle. Complete equilibrium between solid and melt requires very sluggish melt transport, with ascent rates on the order of a few centimeters per year. Complete disequilibrium, on the other hand, requires rapid transport (>30 m yr^{-1}) through a permeable network with channel spacing considerably larger than the grain size. Diffusive fractionation during percolation through depleted spinel peridotite can lead to a wide variety of REE patterns in the melt, depending on the porosity and channel spacing of the melt network. These include ultra-depleted patterns when the porosity is very small (<0.005 for an intergranular network with 2 mm grain radii) and patterns of relative LREE enrichment at moderate porosity (0.02–0.03).

Keywords: mantle; melting; equilibrium; diffusion; rare earths; igneous processes

1. Introduction

The solid and liquid products of adiabatic decompression melting in Earth's upper mantle preserve information on the composition of the mantle, the depth range over which melting takes place, and the mechanisms and rates of melt ex-

* Corresponding author. Present address: Geophysical Laboratory and Department of Terrestrial Magnetism, Carnegie Institution of Washington, 5251 Broad Branch Rd., Washington, DC 20015, USA. Tel.: +1-202-478-8929; Fax: +1-202-478-8901.
E-mail address: j.van_orman@gl.ciw.edu (J.A. Van Orman).

0012-821X/02/$ – see front matter
PII: S0012-821X(02)00492-2

traction. To interpret this information it is necessary to understand how elements are redistributed as melt is produced and transported to the surface. A common assumption in chemical fractionation models is that melting takes place under conditions of local chemical equilibrium. However, it is well known that melt can move rapidly to the surface shortly after it is produced (e.g. [3,4]). In this situation it is important to consider whether there is sufficient time for equilibrium between solid and melt to be achieved, and to evaluate possible kinetic controls on chemical fractionation.

Several models have been developed recently to account for the effects of chemical disequilibrium during partial melting and melt transport [5–13]. Applying these models to melting in Earth's mantle has been an uncertain exercise, due primarily to the lack of experimental data on the kinetics of chemical exchange between solid and melt. The chemical exchange process is controlled by diffusion in the solid, and data on diffusion rates in upper mantle minerals are not abundant, especially for trace elements. Recently we have presented experimental studies of rare earth element (REE) diffusion rates in high-Ca pyroxene [1] and pyrope garnet [2], the two primary hosts of REE in the upper mantle. The availability of these new data sets makes it appropriate to revisit the question of whether chemical equilibrium is maintained during melting and during intergranular melt transport.

In this paper we present a numerical model for trace element fractionation that incorporates the new experimental data for REE diffusion [1,2]. In contrast to previous treatments of disequilibrium melting, which have simplified the problem by treating the solid as a single phase, we consider diffusive exchange between a melt and multiple solid phases, each with different diffusion and partitioning properties. We also consider how elements are redistributed when upwelling mantle crosses the garnet–spinel facies transition, and examine the influence of variations in melt productivity during adiabatic decompression [14].

2. Disequilibrium partial melting model

Partial melting is considered here to take place over a range of depths, in response to adiabatic decompression during mantle upwelling. The terms 'equilibrium' and 'disequilibrium' refer to the progress of chemical exchange reactions between melt and solid that are in intimate contact with each other, and the terms 'batch' and 'fractional' designate two end-member melt segregation processes. 'Equilibrium fractional' melting, for example, refers to the case in which melt is produced in equilibrium with the solid matrix and is removed instantly from further contact with the solid. 'Batch' melting designates a process in which melt always remains in contact with the solid. 'Critical' melting refers to a situation in which a certain fraction of melt remains within the solid matrix, with the rest being removed after a critical melt fraction is exceeded. The melt and solid are in 'disequilibrium' if they do not completely equilibrate chemically while the melt remains in the solid matrix. In the context of the models presented here the core of a mineral grain will be out of equilibrium with the enclosing melt until sufficient time passes to allow diffusion to reequilibrate the mineral from rim to core. 'Complete disequilibrium' melting refers to the case in which there is no chemical exchange between the melt and its enclosing solid matrix, other than that due to dissolution and/or precipitation of solid phases.

2.1. Model formulation

The numerical model presented below simulates diffusion-controlled redistribution of trace elements during partial melting in the upper mantle. The system under consideration is a representative volume of a mantle rock comprising several solid phases. Solid grains are approximated as spheres, and each solid phase is considered to have a uniform grain size. The model simulates the chemical evolution of this idealized system as it ascends and undergoes progressive partial melting due to adiabatic decompression. Partial melting begins when the system encounters the solidus at a pressure P_0 and temperature T_0, and ceases at P_f and

T_f. The first increment of melt is assumed to be a complete disequilibrium (modal) melt whose composition simply reflects the weighted average of the compositions of solid phases that have dissolved to make the melt. This disequilibrium melt is assumed to equilibrate instantaneously with the contact surfaces of the solid grains, inducing chemical gradients within the grains that

Table 1
Notation

Variable	Description	Dimension
b	Constant in permeability	None
C_j^i	Concentration of element i within solid phase j	kg m^{-3}
$C_{j,0}^i$	Concentration of element i within solid phase j before melting begins	kg m^{-3}
C_m^i	Concentration of element i within the residual melt	kg m^{-3}
C_M^i	Concentration of element i within the pooled extracted melt	kg m^{-3}
D_j^i	Diffusion coefficient of element i within solid phase j	m^2 s^{-1}
$D_{o,j}^i$	Pre-exponential factor for diffusion of element i within solid phase j	m^2 s^{-1}
$\mathcal{E}_j^i$	Zero-pressure activation enthalpy for diffusion of element i within solid phase j	J mol^{-1}
f	Fraction of melting	None
F	Total fraction of melting at the top of the melting column	None
g	Gravitational acceleration	m s^{-2}
H	Height of melting column	m
k	Permeability = $R^2\phi^n/4b$	m^2
K_j^i	Mineral/melt equilibrium partition coefficient for element i	None
n	Exponent in permeability	None
N_j	Number of grains of solid phase j	Pa
P	Pressure	Pa
P_0	Pressure when melting begins	Pa
P_f	Pressure when melting stops	Pa
$P_{gt\rightarrow sp}$	Pressure of the garnet to spinel facies transition	Pa
r_j	Radial coordinate within solid phase j	m
$\mathcal{R}$	Gas constant	J mol^{-1} K^{-1}
R_j	Radius of a grain of solid phase j	m
$R_{j,0}$	Initial radius of a grain of solid phase j (before melting begins)	m
t	Time	s
T	Temperature	K
T_0	Temperature when melting begins	K
T_f	Temperature when melting stops	K
$T_{gt\rightarrow sp}$	Temperature at the garnet to spinel facies transition	K
V_0	Volume of solid before melting begins	m^3
$\mathcal{V}_j$	Volume of solid phase j	m^3
V_m	Volume of residual melt	m^3
V_M	Volume of pooled extracted melt	m^3
$\mathcal{V}_j^i$	Activation volume for diffusion of element i within solid phase j	m^3 mol^{-1}
w	Melt velocity	m s^{-1}
W	Solid matrix velocity	m s^{-1}
X_j	Volume fraction of solid phase j	None
$X_{j,0}$	Volume fraction of solid phase j before melting begins	None
z	Vertical coordinate	m
α_j	Stoichiometric coefficient of solid phase j in melting reaction	None
ϕ	Porosity	None
ϕ_{crit}	Critical porosity	None
μ	Melt shear viscosity	Pa s
$\Delta\rho$	Density difference between matrix and melt	kg m^{-3}
υ_e	Melt extraction rate	m^3 s^{-1}
υ_m	Melting rate	m^3 s^{-1}

are relaxed with time by solid-state diffusion. The extent to which the solid grains and melt are able to equilibrate as partial melting proceeds depends on the ratio of the diffusive relaxation time to the time required for production and extraction of melt from the solid matrix.

The system is composed of several distinct reservoirs – each solid phase that hosts the trace elements of interest, the residual melt that remains within the solid matrix, and the aggregated melt formed by continuous extraction of melt from the matrix. Melt is assumed to remain with the solid matrix until a critical melt fraction is reached, after which melt is extracted so that the porosity remains constant. Once melt is extracted it is assumed to undergo no further chemical interaction with the solid phases.

The concentration of a chemical species i within a spherical grain of solid phase j is given by Fick's second law (in spherical coordinates):

$$\frac{\partial C_j^i}{\partial t} = D_j^i\left(\frac{\partial^2 C_j^i}{\partial r_j^2} + \frac{2}{r_j}\frac{\partial C_j^i}{\partial r_j}\right) \tag{1}$$

where $C_j^i = C_j^i(r_j,t)$ is the concentration at a distance r_j from the center of the grain. A complete list of model parameters and their dimensions is provided in Table 1. The diffusion coefficient D_j^i is considered to have an Arrhenian dependence on temperature and pressure:

$$D_j^i = D_{0,j}^i \exp\left(\frac{-(\mathcal{E}_j^i + P\,\mathcal{V}_j^i)}{\mathcal{R}T}\right) \tag{2}$$

Boundary conditions for Eq. 1 are based on the following assumptions: (1) before melting begins, there is no compositional zoning within the solid grains and (2) chemical species are distributed among the solid phases in equilibrium proportions; (3) during melting, chemical equilibrium between the residual melt and the *surfaces* of solid grains is maintained at all times. These boundary conditions are expressed by the following equations:

$$C_j^i|_{t=0} = C_{j,0}^i \tag{3}$$

$$\frac{C_{j1,0}^i}{K_{j1}^i} = \frac{C_{j2,0}^i}{K_{j2}^i} = \ldots \frac{C_{jn,0}^i}{K_{jn}^i} \tag{4}$$

$$C_j^i|_{r_j=R_j} = K_j^i C_{\mathrm{m}}^i \tag{5}$$

$$\left.\frac{\partial C_j^i}{\partial r_j}\right|_{r_j=0} = 0 \tag{6}$$

where K_j^i is the equilibrium mineral/melt partition coefficient and $c^i{}_{\mathrm{m}}$ is the concentration of chemical species i in the residual melt.

The mass balance equation for a chemical species in the residual melt is:

$$\frac{\mathrm{d}(V_{\mathrm{m}} C_{\mathrm{m}}^i)}{\mathrm{d}t} = \sum_j -N_j 4\pi (R_j)^2 D_j^i \left.\frac{\partial C_j^i}{\partial r_j}\right|_{r_j=R_j} +$$

$$\sum_j \upsilon_{\mathrm{m}} \alpha_j C_j^i|_{r_j=R_j} - \upsilon_{\mathrm{e}} C_{\mathrm{m}}^i \tag{7}$$

$$= -\frac{\mathrm{d}}{\mathrm{d}t}\left\{\sum_j N_j \int_0^{R_j} 4\pi (r_j)^2 C_j^i \mathrm{d}r_j\right\} - \upsilon_{\mathrm{e}} C_{\mathrm{m}}^i \tag{8}$$

where V_{m} is the volume of residual melt, R_j is the time-dependent radius of solid grain of phase j, N_j is the number of grains of phase j in the system, υ_{m} and υ_{e} are the volumetric melting and melt extraction rates, respectively, and α_j is the stoichiometric coefficient of phase j in the melting reaction. By using volume to keep track of melt production we have not rigorously kept track of the mass redistribution unless the melt and solid have equal densities. In the case of mantle minerals and melts this simplification will not lead to significant differences at low melt fractions (1–2%) and at the highest melt fractions considered in this paper (20%) absolute abundances will be in error by only 2–4%. The terms on the right-hand side of Eq. 7 represent, in order: the total diffusive current of a chemical species across the interface between the melt and each solid phase; mass transfer from solid to melt due to phase change (dissolution/precipitation); and removal of a chemical species from the residual melt by melt extraction. In Eq. 8 the diffusion and dissolution

terms are combined within the integral. This equation is used instead of Eq. 7 because the integrated concentration of an element in a solid grain can be calculated far more accurately than the concentration gradient at the rim of the grain [5,12].

Mass balance in the pooled extracted melt is given by the equation:

$$\frac{\mathrm{d}V_{\mathrm{M}}C^{i}_{\mathrm{M}}}{\mathrm{d}t} = \upsilon_{\mathrm{e}}C^{i}_{\mathrm{m}} \tag{9}$$

where C^{i}_{M} is the concentration of element i in the extracted melt and V_{M} is the volume of extracted melt. Both the residual and pooled extracted melts are assumed to be compositionally homogeneous at all times. This assumption is justified for the residual melt because chemical diffusion rates in silicate melts are much faster than in silicate minerals and because the length scale over which diffusion must take place is relatively small (a centimeter or less for melt distributed along three-grain junctions in peridotite). For example, diffusion of Nd at 1300°C ($D \approx 10^{-11}$ m^2/s [15]) is rapid enough to homogenize a basaltic melt on a centimeter length scale in about 1 year, which is very short compared to the $\sim$My time scale of melting beneath mid-ocean ridges. Homogenization of the aggregated melt is not assured, as it will depend on the geometry and size of the melt reservoir and on the vigor of convective mixing within it. However, the chemical distribution within the aggregated melt has no bearing on the chemical evolution of other parts of the system (residual melt and solid phases), and the concentration of a chemical species in the aggregated melt simply represents the integrated concentration in this reservoir.

The melting rate, in m^3/s, is given by:

$$\upsilon_{\mathrm{m}} = V_0 W \frac{\partial F}{\partial z} \tag{10}$$

where V_0 is the initial solid volume, defined as $\sum_j N_j 4/3\pi(R_{j,0})^3$, W is the upwelling velocity, and $(\partial F/\partial z)$ is the melt productivity, or the fraction of melt produced per meter of adiabatic ascent. In most of the calculations to follow υ_{m} is taken to be constant, but we also examined the more realistic case in which the melt productivity increases during melting as proposed by Asimow et al. [14].

With progressive melting, the volume of each solid phase changes according to:

$$\frac{\mathrm{d}V_j}{\mathrm{d}t} = -\alpha_j \upsilon_{\mathrm{m}}$$

where α_j is the stoichiometric coefficient of phase j in the melting reaction. Solid grains are assumed to melt from their outer rims, preserving their spherical symmetry as they dissolve, and the number of grains within the system is assumed to remain constant (i.e. no new grains nucleate, and grains do not coalesce). Given these assumptions, the radius of each solid grain changes with time according to:

$$R_j = R_{j,0}\left(1 - \frac{\upsilon_{\mathrm{m}}\alpha_j t}{V_0 X_{j,0}}\right)^{1/3} \tag{11}$$

when υ_{m} is constant.

The rate of melt extraction from the solid matrix, υ_{e}, is initially zero. When the melt fraction exceeds the critical porosity ϕ_{crit} it is given by:

$$\upsilon_{\mathrm{e}} = \frac{1}{1-\phi_{\mathrm{crit}}}\upsilon_{\mathrm{m}} \tag{12}$$

Thus the melt segregation rate is treated as a simple step function in which melt remains within the solid matrix until a critical porosity is reached and thereafter is removed at the rate described by Eq. 12. Although this simple functional form may not perfectly represent the actual melt segregation process, it does encompass the end-members of fractional ($\phi_{\mathrm{crit}} = 0$) and batch ($\phi_{\mathrm{crit}} = F$) melting and allows for straightforward comparisons between the present model and equilibrium trace element distribution models in common use.

Eqs. 1–12 are solved numerically using a fully implicit Crank–Nicolson finite difference algorithm. At each time step, the concentration of an element in the residual melt and the concentration distribution within each solid grain are calculated simultaneously. For each solid grain a fixed number of radial grid points is maintained throughout the calculation, and the moving boundary is accommodated by re-scaling the

grid to the new grain radius R_j at each time step. The numerical algorithm is unconditionally stable, and at the limits of very large and very small D_j^i it recovers the analytical solutions for complete equilibrium and complete disequilibrium melting, respectively. The accuracy of the calculations was assessed by checking mass balance of a chemical species among the solid, residual melt, and aggregated melt at each time step, and by comparing the results of calculations using different grid spacings. Mass balance is achieved within less than 1.3% relative for the grid used in most of the calculations (40 radial steps for each solid grain and 320 time steps). Use of finer grid spacings leads to changes of less than a few percent in the calculated compositions of residual melt, pooled melt, and solid phases.

2.2. Assumptions

Several assumptions have been made in constructing this model, the most important of which concern the chemical exchange process, the mechanical integrity of the solid grains, and the boundary condition at the interface between solid grains and residual melt. Chemical exchange between solid and melt is considered to result only from diffusion and from the incremental dissolution of mineral grains as partial melting proceeds. Solid grains are assumed to maintain their mechanical integrity, with no internal deformation and no motion of grain or phase boundaries other than that due to steady dissolution of a solid phase into the melt. Deformation must of course take place as the mantle ascends, and associated recrystallization processes might significantly enhance the rate of chemical exchange. However, high-Ca pyroxene and garnet, the principal hosts of incompatible elements in the upper mantle, have considerably higher shear strength than the more abundant minerals olivine and orthopyroxene (opx) [16–20] and thus may be expected to undergo little deformation. Also, recrystallization of these minerals by grain boundary migration is probably not important because each composes a relatively small fraction of the upper mantle – few garnet–garnet and clinopyroxene (cpx)–cpx grain boundaries exist. We therefore consider it a reasonable assumption that most of the deformation associated with mantle upwelling is accommodated by opx and olivine, with garnet and cpx behaving as essentially rigid grains.

Another important assumption of the model is that the entire outer boundary of each solid grain is in equilibrium with the residual melt. Because silicate melts probably are not in contact with the entire outer boundary of solid grains, residing instead at three-grain junctions (e.g. [21]), satisfying this condition means that grain boundary diffusion must be rapid enough to allow all parts of the boundary to maintain communication with the residual melt. In the absence of grain boundary diffusion, equilibrium would be maintained only over the small portion of the surface where the grain and the melt are in physical contact, and the rate of diffusive exchange between solid and melt would be significantly reduced. The available data for polycrystalline olivine and enstatite [22,23] indicate that grain boundary diffusion rates are on the order of 10^{-12} m^2/s at temperatures close to the solidus of peridotite. Given a diffusivity of this order, only a few years is required to transport ions along a grain boundary connecting melt tubules separated by 1 cm. This time is short compared to typical time scales for melting and melt extraction in the mantle, and thus the assumption that solid grains are in equilibrium with residual melt over their entire boundary appears to be justified.

3. Diffusive fractionation of REE during melting

The REE are among the most widely used tracers of partial melting processes in the upper mantle, and because their diffusion rates in cpx are known to vary widely and systematically with ionic radius [1] they represent an ideal case for examining the effects of diffusive fractionation during melting. In this section we demonstrate the conditions under which diffusive fractionation of REE may take place and show how the melting rate, solid grain size, and efficiency of melt extraction may influence REE abundance patterns in the solid and liquid products of partial melting.

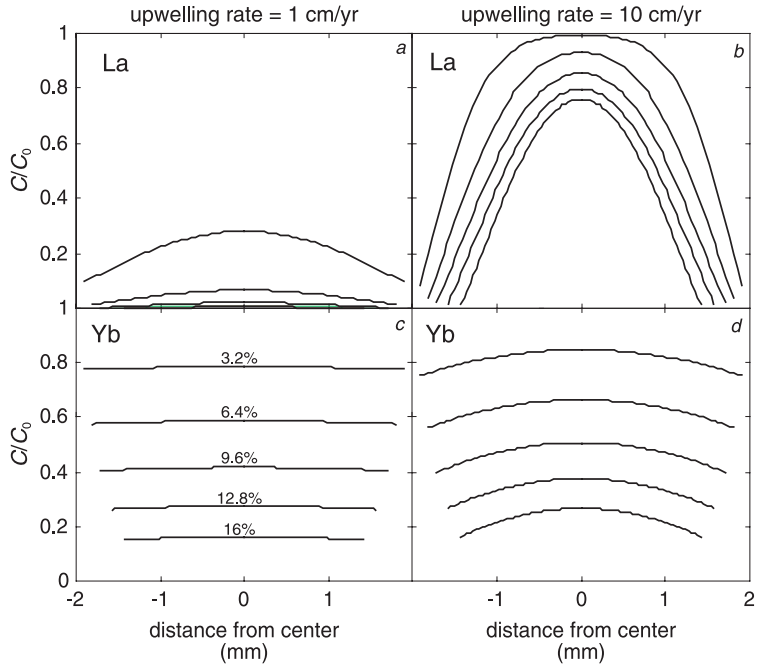

Fig. 1. Model diffusion profiles developed within a 2 mm radius cpx grain during progressive melting within the spinel stability field, beginning at 2.0 GPa, 1400°C and ceasing at 0.4 GPa, 1240°C. Each panel shows rim-to-rim diffusion profiles at five equally spaced melting increments (3.2%, 6.4%, 9.6%, 12.8% and 16%). (a,c) La and Yb profiles, respectively, for an upwelling rate of 1 cm yr^{-1}. (b,d) La and Yb profiles for an upwelling rate of 10 cm yr^{-1}. $\partial F/\partial P = 0.1$ GPa^{-1}, $F = 0.16$, $\phi_{crit} = 0.01$.

Table 2
Partition coefficients, diffusion parameters, and initial bulk concentration

	K_{cpx} [a]	K_{opx} [a]	K_{gt} [a]	$D_{0,cpx}$ [b] (m^2 s^{-1})	$D_{0,gt}$ (m^2 s^{-1})	$\mathcal{E}_{cpx}$ [b] (kJ mol^{-1})	$\mathcal{E}_{gt}$ (kJ mol^{-1})	$\mathcal{V}_{cpx}$ (m^3 mol^{-1})	$\mathcal{V}_{gt}$ (m^3 mol^{-1})	$\mathcal{C}_0$ [c]
La	0.054	5e-4	1e-3	4.20e-3	2.34e-9	519.3	287.7	1e-5	1e-5	0.296
Ce	0.086	9e-4	4e-3	2.20e-3	2.34e-9	508.2	287.7	1e-5	1e-5	0.361
Nd	0.19	9e-3	0.06	5.54e-4	2.34e-9	483.9	287.7	1e-5	1e-5	0.482
Sm	0.29	0.02	0.5	1.42e-4	2.34e-9	460.1	287.7	1e-5	1e-5	0.593
Dy	0.44	0.06	2.5	9.97e-6	2.34e-9	413.6	287.7	1e-5	1e-5	0.770
Er	0.44	0.07	3	2.73e-6	2.34e-9	390.9	287.7	1e-5	1e-5	0.785
Yb	0.43	0.1	4	8.83e-7	2.34e-9	371.2	287.7	1e-5	1e-5	0.800

[a] Mineral/melt equilibrium partition coefficients [24,25].

[b] D_0, $\mathcal{E}$ and $\mathcal{V}$ values for cpx are interpolated using the elastic model discussed in [1]. These values reproduce experimentally determined diffusion coefficients for La, Ce, Nd, Dy and Yb in diopside within a factor of two at temperatures from 1050 to 1450°C and pressures from 0.1 MPa to 2.5 GPa [1]. D_0, E and $\mathcal{V}$ values for garnet reproduce experimental diffusion coefficients for Ce, Sm, Dy and Yb within a factor of two at 2.8 GPa and 1200–1450°C [2]. $\mathcal{V}$ for garnet is assumed, but its exact value is not critical because garnet is present only within a small pressure range in the mantle melting regime.

[a] Initial concentrations in the bulk solid. Relative abundances reflect the values estimated by Shimizu [26] for depleted MORB mantle.

3.1. Melting in the spinel stability field

We first consider models in which melting begins in the spinel stability field. High-Ca pyroxene is the primary host of REE in spinel lherzolite, and in the calculations discussed here this phase is assumed to contain all of the REE in the solid matrix. We have also performed calculations in which opx as well as cpx is allowed to exchange REE with the melt. Regardless of the diffusion properties assumed for opx, the results do not differ greatly from those in which the opx partition coefficients are assumed to be zero, because the initial opx contains such a small proportion of the total REE budget.

The partition coefficients and diffusion parameters used in making the calculations are listed in Table 2. The initial proportions of solid phases in the system and the proportions in which the solid phases enter the melt during partial melting (i.e. the melt reaction coefficients) are listed in Table 3. We assume that for each solid phase the melt reaction coefficient and partition coefficients remain constant throughout the melting process. Although cpx/melt partition coefficients are known to vary with pressure, temperature and composition (e.g. [25,29,30]), there are only small changes in the relative values of REE partition coefficients. Our primary interest here is in examining the influence of diffusion on fractionation of the REE, and for this purpose it is convenient to assume constant partition coefficients. Also, while reaction coefficients may change as melting progresses, cpx always dominates the melt mode [31–34] and its reaction coefficient does not vary greatly. The relative proportions of opx and olivine dissolving into or crystallizing from the melt do vary significantly with pressure [27], but this has no bearing on the present model because neither opx nor olivine is a significant host of REE. For the present purposes, all solid phases other than cpx can be treated as a single barren phase with a constant melt reaction coefficient.

Figs. 1 and 2 show the results of a series of calculations that simulate diffusive REE exchange during adiabatic decompression melting within a one-dimensional mantle column. In these calculations the solidus is intersected at a pressure of 2.0 GPa and temperature of 1400°C, and the temperature decreases linearly at 100°C GPa^{-1} until melting ceases at 0.4 GPa and 1240°C [31]. The diffusion coefficient for each element depends on temperature and pressure (Table 2) and decreases by approximately an order of magnitude from the bottom of the melting column to the top. In these calculations the melt productivity is assumed to have a constant value of 0.1 GPa^{-1}, leading to a total melting fraction of 16% at the top of the column. The melting rate is directly proportional to the solid upwelling rate W. We have chosen to present the results in terms of a common initial grain radius of 2 mm, and to vary the degree of disequilibrium by changing the upwelling rate. There is a linear correspondence between the upwelling rate (which determines the time scale of the calculation) and the square of the grain size (which determines the length scale of diffusion), and this can be used to extend the results presented in the figures below to other initial grain radii. Increasing the upwelling rate by a factor of four, for example, is equivalent to increasing the initial grain size by a factor of two.

Fig. 1 shows La and Yb diffusion profiles developed within a cpx grain, initially 2 mm in radius, with progressive melting. Lanthanum is the most incompatible of the REE and has the most

Table 3
Phase proportions

Phase	Initial solid spinel facies[a]	Initial solid garnet facies	Melt mode spinel facies	Melt mode garnet facies[b]
Cpx	0.20	0.20	0.80	0.80
Opx	0.24	–	0.30	–
Garnet	0	0.08	–	0.30
Other	0.56	0.72	−0.10	−0.10

[a] Phase proportions for depleted MORB mantle in spinel facies [27].
[b] Garnet facies melt mode from melting reactions at 3.0 GPa [28].

sluggish diffusion kinetics; Yb is only moderately incompatible and diffuses ~30 times more rapidly than La. At upwelling rates of 1 cm yr^{-1} (typical of passive upwelling beneath a slow spreading ridge) and 10 cm yr^{-1} (typical of a fast spreading ridge) Yb concentration profiles are nearly flat, indicating that Yb is distributed in near equilibrium proportions between the solid and residual melt. Lanthanum, on the other hand, is moderately zoned even at an upwelling rate of 1 cm yr^{-1}, and at 10 cm yr^{-1} is very strongly zoned. Thus, under conditions typical of melting beneath mid-ocean ridges, La may be extracted from the solid much less efficiently than under conditions of complete grain-scale equilibrium, while Yb diffuses rapidly enough to be near equilibrium with the melt.

Fig. 2 shows the influence of diffusion-controlled exchange on the REE patterns in the solid (Fig. 2a) and aggregated melt (Fig. 2b) after near fractional partial melting is complete. The REE patterns are bracketed by the solutions for complete equilibrium and complete disequilibrium (no diffusive exchange between cpx and melt), which are shown as bold lines. The composition of the solid after melting at complete disequilibrium (Fig. 2a) differs from that of the initial solid because melting is non-modal, with cpx composing 80% of the melt. At upwelling rates as slow as 0.3 cm yr^{-1} the REE pattern in the residual solid begins to diverge significantly from that of a solid depleted by equilibrium near fractional melting, and at upwelling rates greater than 100 cm yr^{-1} the residue composition approaches that of a solid produced by complete disequilibrium melting. Because light REE are affected at much lower upwelling rates than heavy REE, the REE patterns shallow significantly as the upwelling rate increases (Fig. 2a).

The aggregated melt is less sensitive than the residual solid to disequilibrium partitioning of incompatible elements, and does not show the effects of diffusion-controlled exchange unless the upwelling rate exceeds ~3 cm yr^{-1} (Fig. 2b). As the upwelling rate increases beyond this threshold value, the concentrations of REE decrease, but in contrast to the residual solid there is almost no change in the shape of the REE pattern. This is a consequence of two competing factors: the increase in diffusivity across the lanthanide series, and the insensitivity of large degree aggregated melts to variations in the effective partitioning of highly incompatible elements. The concentration of a highly incompatible element in the aggregated melt changes significantly only when its effective partition coefficient exceeds the melting fraction (in this case 0.16). For the light REE such a change in effective partitioning requires a large degree of disequilibrium. The mod-

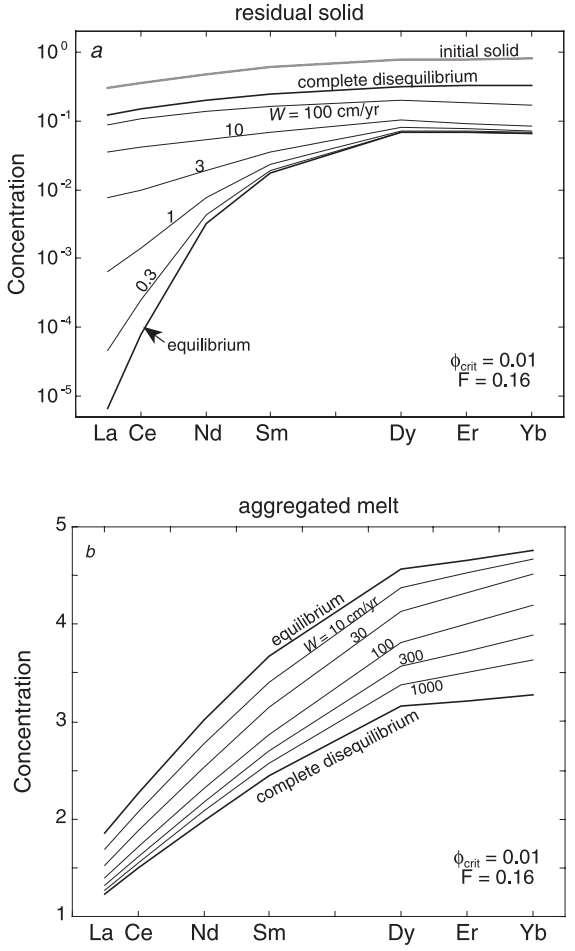

Fig. 2. Influence of upwelling rate on the REE compositions of the residual solid (a) and aggregated melt (b) after 16% near fractional melting in the spinel stability field. Numbers on curves indicate upwelling rates in cm yr^{-1}. Initial grain radius is 2 mm, $\phi_{crit} = 0.01$.

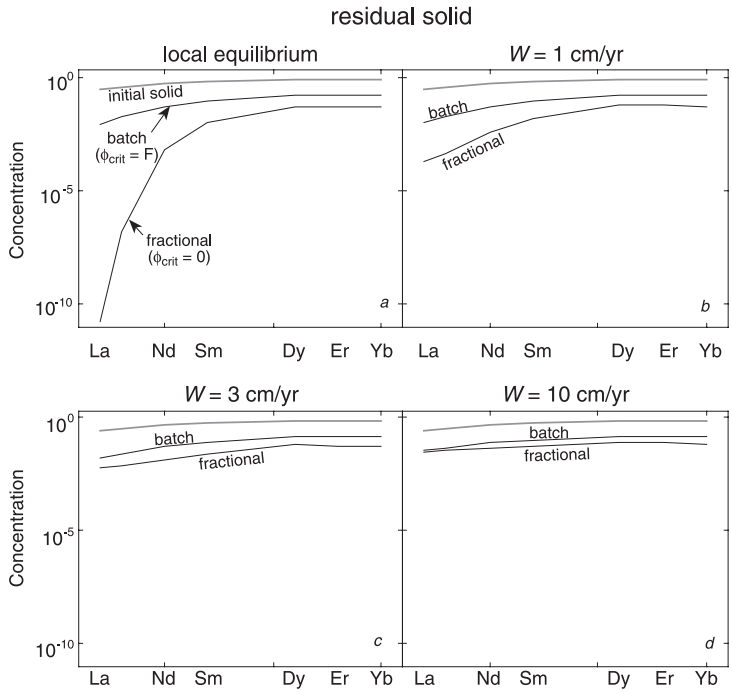

Fig. 3. Influence of residual porosity on the composition of the residual solid after 16% melting, under the condition of local equilibrium (a) and for various degrees of disequilibrium (b–d). With increasing deviation from equilibrium, the solid residue of fractional melting ($\phi_{crit} = 0$; instantaneous melt extraction) becomes more similar in composition to that produced by batch melting ($\phi_{crit} = F$; no melt extraction). The La concentration after 16% batch melting is higher by a factor of $\sim 10^8$ than for fractional melting, if local equilibrium is achieved; the difference is less than a factor of two for disequilibrium melting at an upwelling rate of 10 cm yr^{-1} (d). Initial grain radius is 2 mm.

erately incompatible heavy REE are much more sensitive to variations in effective partitioning, and begin to show the effects of disequilibrium partitioning when the deviation from equilibrium is relatively small. If diffusion rates among the REE were uniform, then with increasing upwelling rate the REE patterns in the aggregated melt would decrease in slope, reflecting the difference in behavior of highly and moderately incompatible elements. The increase in diffusivity across the lanthanide series happens to be just sufficient to offset this effect and keep the slope of the REE pattern nearly constant. An unfortunate consequence of this is that it makes diffusion-controlled exchange of REE during partial melting difficult to detect in high-degree aggregated melts like mid-ocean ridge basalts. The REE composition of a disequilibrium aggregated melt is difficult to distinguish from that of an equilibrium aggregated melt produced by a higher degree of partial melting or by melting of a more depleted source.

The efficiency of melt extraction, represented by the parameter ϕ_{crit}, has a strong influence on the chemical evolution of the residual solid under conditions of local equilibrium, but its importance diminishes as the deviation from equilibrium increases (Fig. 3). Incompatible elements are removed from the solid most efficiently if solid and melt are in equilibrium and melt is extracted continuously as soon as it is produced (equilibrium fractional melting). Depletion is less efficient if some or all of the melt is retained within the solid matrix, or if diffusion limits the exchange of elements between solid and melt; inefficient melt removal and inefficient diffusive exchange have similar effects on the chemical evolution of the solid. With increasing degree of disequilibrium, the

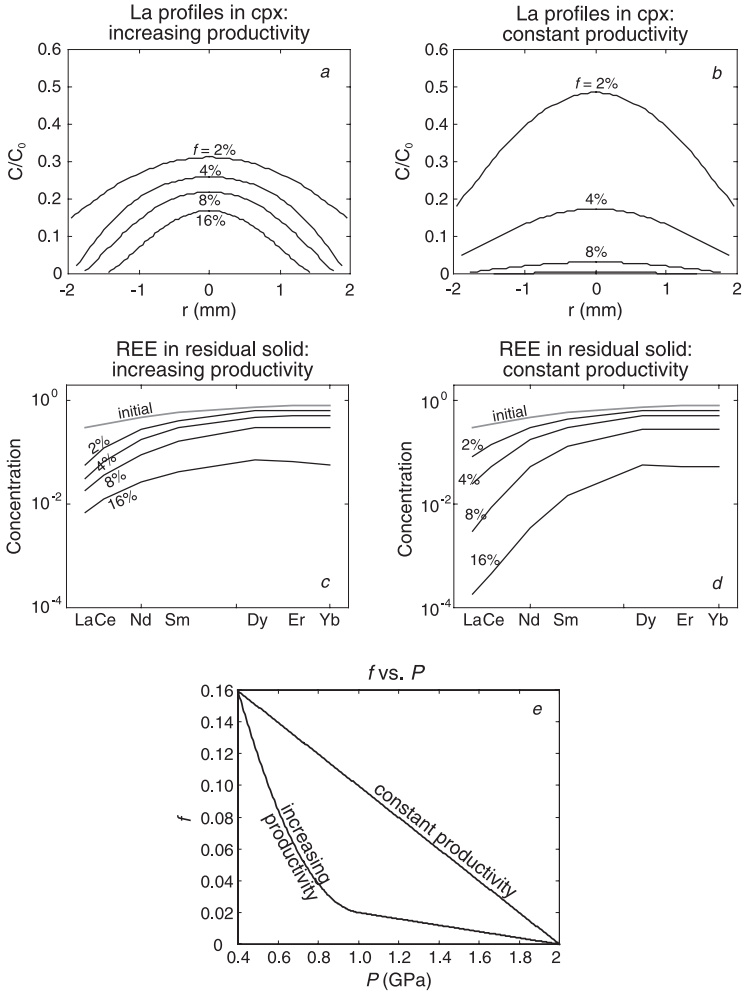

Fig. 4. Influence of melt productivity ($\partial f/\partial P$) on the chemical evolution of the residual solid. La diffusion profiles in cpx (a,b) and the integrated REE composition of the residual solid (c,d) are shown for the increasing productivity and constant productivity functions illustrated in panel e. In the case of increasing productivity, equilibration is favored at low extents of melting ($<3\%$) but is hindered at higher melting degrees. The calculations shown are for $\phi_{crit}=0$, $R_0=2$ mm, and $W=1$ cm yr^{-1}, but general aspects of the chemical evolution are similar for other parameter values.

composition of a solid produced by fractional melting approaches that of a solid produced by batch melting (Fig. 3). In the end-member case of complete disequilibrium the chemical evolution of the residual solid is completely insensitive to the extraction of melt, and there is no distinction between batch and fractional melting.

3.2. Influence of variations in melt productivity

In the calculations discussed above the melt productivity ($\partial f/\partial P$) was assumed to be constant. As discussed by Asimow et al. [14,35] the melt productivity is likely to vary significantly during adiabatic decompression melting. For near fractional melting beginning within the spinel stability field, productivity is predicted to remain nearly constant up to 1.0 GPa ($\sim$30 km depth) and to increase sharply as the mantle ascends to lower pressures [14]. To examine the influence of variable melt productivity on the distribution of the REE we have performed a set of calculations in

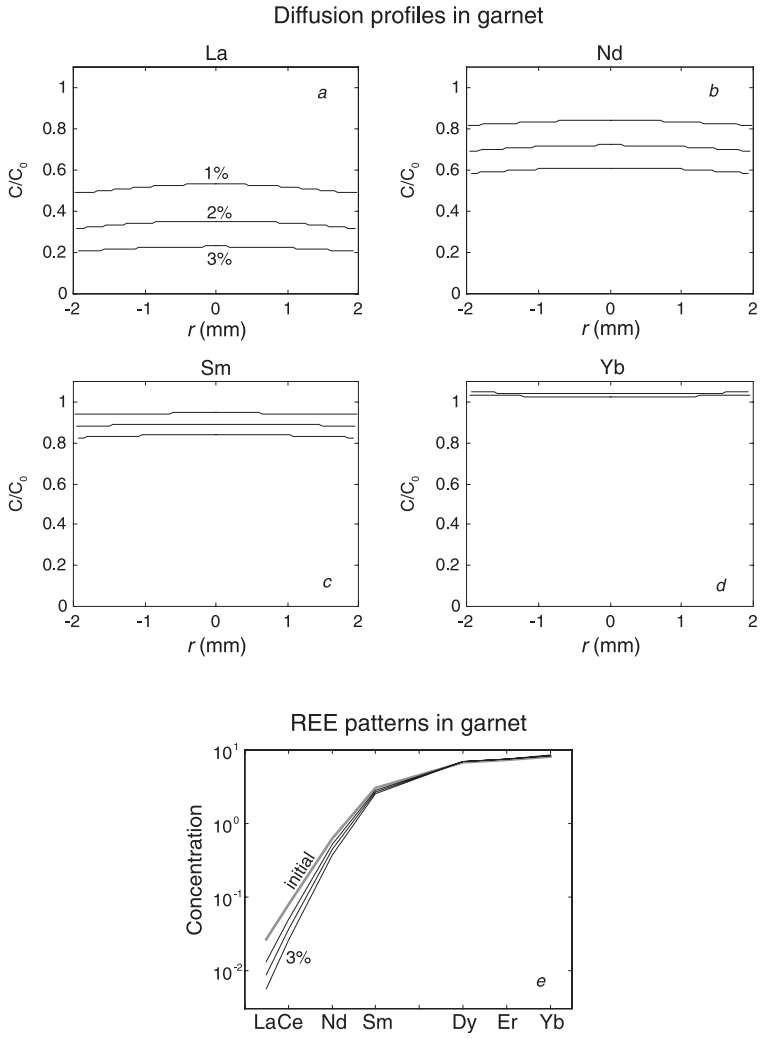

Fig. 5. Chemical evolution of garnet during partial melting in the garnet stability field between 2.8 and 2.5 GPa. Diffusion profiles for La, Nd, Sm and Yb are shown in panels a–d, and the integrated REE composition of garnet is shown in panel e. For the upwelling rate (3 cm yr^{-1}), initial grain radius (2 mm), and residual porosity (0.01) used in the calculations, garnet is near equilibrium with the residual melt.

which the productivity is held constant, at 0.02 GPa^{-1}, between 2.0 and 1.0 GPa, and then increases linearly at 0.717 GPa^{-2} from 1.0 to 0.4 GPa. The total degree of melting at the top of the melting column is the same as in the calculations above (16%). Fig. 4 shows how the chemical evolution of the residual solid differs from the case in which the melt productivity is constant. During the early stages of melting the productivity is low and REE are removed efficiently from the solid, but as melting proceeds the degree of disequilibrium increases sharply and removal of REE from the solid becomes increasingly difficult. At low extents of melting ($\sim$2% or less) the solid is depleted more efficiently than in the case of constant productivity, but at higher degrees of melting the reverse is true. In the calculations shown in Fig. 4, the crossover in relative depletion between the two productivity functions occurs at less than 4% melting. Although the results shown in Fig. 4 are for the specific case of fractional melting of a solid with initial grain radius of

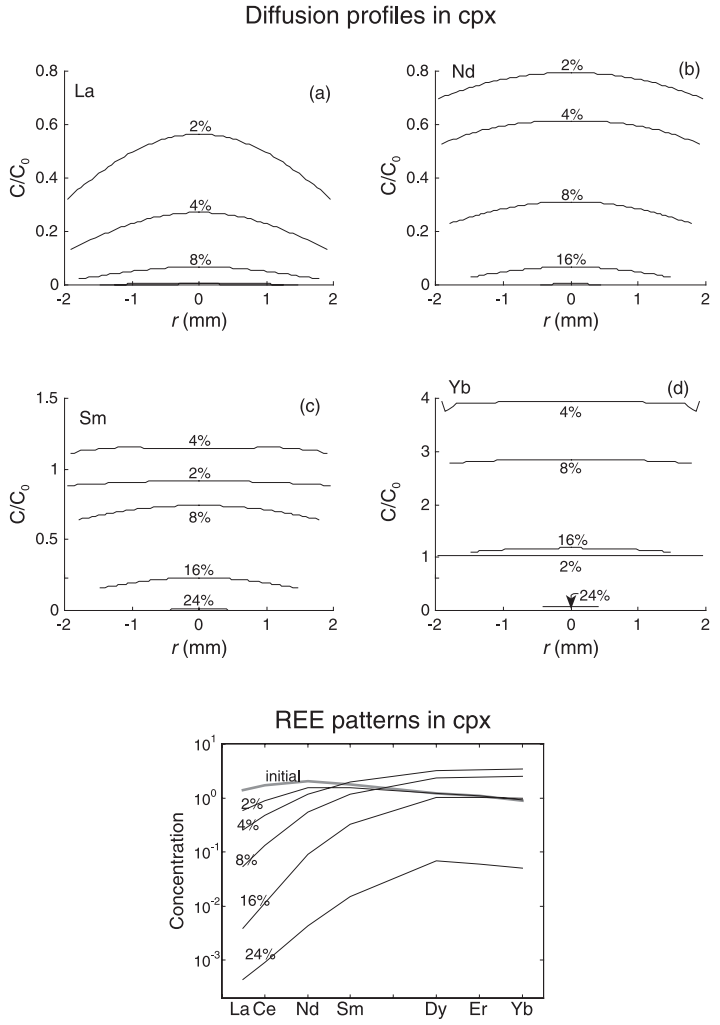

Fig. 6. Diffusion profiles (a–d) and REE patterns (e) in cpx during progressive melting beginning in the garnet stability field at 2.8 GPa. 3% melting takes place in the presence of garnet, with an additional 21% melting in the spinel stability field. Garnet has little influence on the chemical evolution of La (a) and Nd (b), but exerts a strong control on the abundances of Sm (c) and Yb (d) in cpx. Abundances of Sm, Yb, and other middle and heavy REE in cpx increase abruptly at the garnet–spinel transition when all of the REE that were stored in garnet are released instantly into the residual melt. $R_0 = 2$ mm, $W = 3$ cm yr^{-1}, $\phi_{crit} = 0.01$.

2 mm, at an upwelling rate of 1 mm yr^{-1}, the general aspects of the chemical evolution are similar for other grain sizes, upwelling rates, and residual porosities. We have found no conditions under which the increasing productivity function depletes the solid of REE more effectively than constant productivity, at degrees of melting greater than $\sim$10%.

3.3. Melting in the garnet stability field

We now extend the model to situations in which melting begins in the garnet stability field, at depths greater than 75 km, and continues into the spinel stability field at shallower depths. Before melting begins the REE are partitioned in equilibrium between garnet and cpx, and after

the solidus is crossed both solid phases exchange REE with the melt. When the upwelling mantle encounters the garnet–spinel facies boundary, garnet and olivine react to produce pyroxenes and spinel until garnet is exhausted from the residue. Cpx is a reaction product during the transformation to the spinel-facies assemblage, but in reasonable bulk compositions the amount of cpx produced will be small. We ignore any new cpx that is produced as the boundary is crossed and consider the number of cpx grains to remain constant. At the garnet–spinel transition, it is assumed that all of the REE within garnet grains are released instantly into the residual melt. Cpx grains then undergo diffusion-controlled exchange with this new, more enriched melt. Under subsolidus conditions, opx may inherit elevated abundances of REE from the garnet reactant [36], but we expect that when melt is present it will dissolve the bulk of the REE. We also assume that the melt productivity remains constant across the garnet–spinel transition, although in reality it must drop significantly [35].

Figs. 5–7 illustrate the chemical evolution of a system undergoing near fractional melting beginning in the garnet stability field at 2.8 GPa and 1480°C. In this example, 3% melting takes place in the presence of garnet, and an additional 21% melting takes place in the spinel stability field. The initial grain radius is 2 mm for both cpx and garnet, and the upwelling rate is 3 cm yr^{-1}. REE diffusion rates in garnet are similar to heavy REE diffusion rates in cpx under the *T–P* conditions of interest, and garnet is near equilibrium with the residual melt (Fig. 5). The presence of garnet has a strong influence on the chemical evolution of co-existing cpx (Fig. 6). Heavy REE are compatible in garnet, and while garnet remains in the residue cpx exhibits a characteristic 'humped' REE pattern with low relative concentrations of heavy REE (Fig. 6e). When the garnet–spinel boundary is crossed the concentrations of heavy REE in the residual melt increase abruptly, but the light REE, which are highly incompatible in garnet, are affected very little (Fig. 7). In response to the dissolution of garnet, heavy REE concentrations in cpx increase just after the garnet–spinel boundary is crossed, and as melting continues the high relative concentrations of heavy REE in cpx and residual melt gradually diminish.

3.4. Comparison with abyssal peridotite data

As noted above, the residual solid is more sensitive than the aggregated melt to diffusion-limited chemical exchange of incompatible elements during partial melting. Thus, despite the much larger chemical data set for basalts, abyssal peridotites are a better place to look for signatures of disequilibrium melting. The most useful information would come from high spatial resolution compositional data within residual cpx grains. The pres-

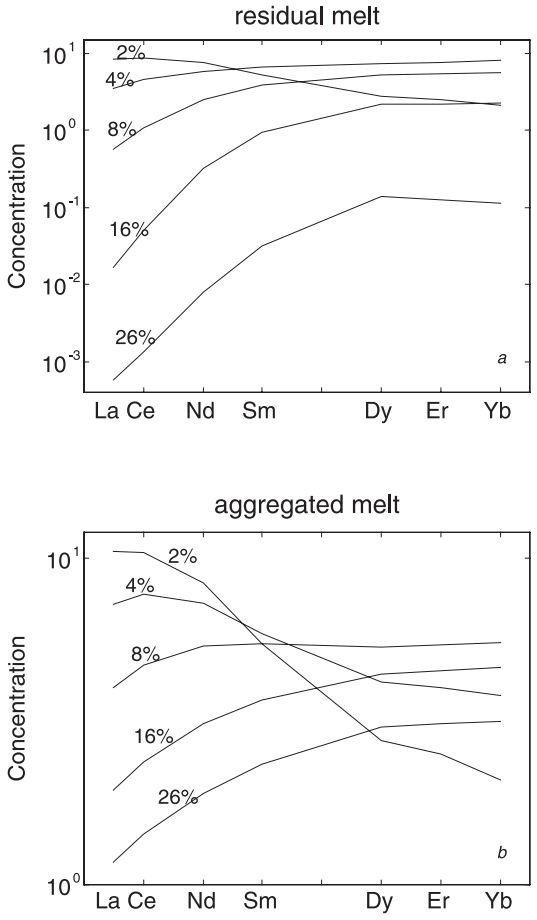

Fig. 7. REE compositions of the (a) residual and (b) aggregated melts produced during partial melting across the garnet–spinel transition, between 2.8 and 0.4 GPa. $R_0 = 2$ mm, $W = 3$ cm yr^{-1}, $\phi_{crit} = 0.01$.

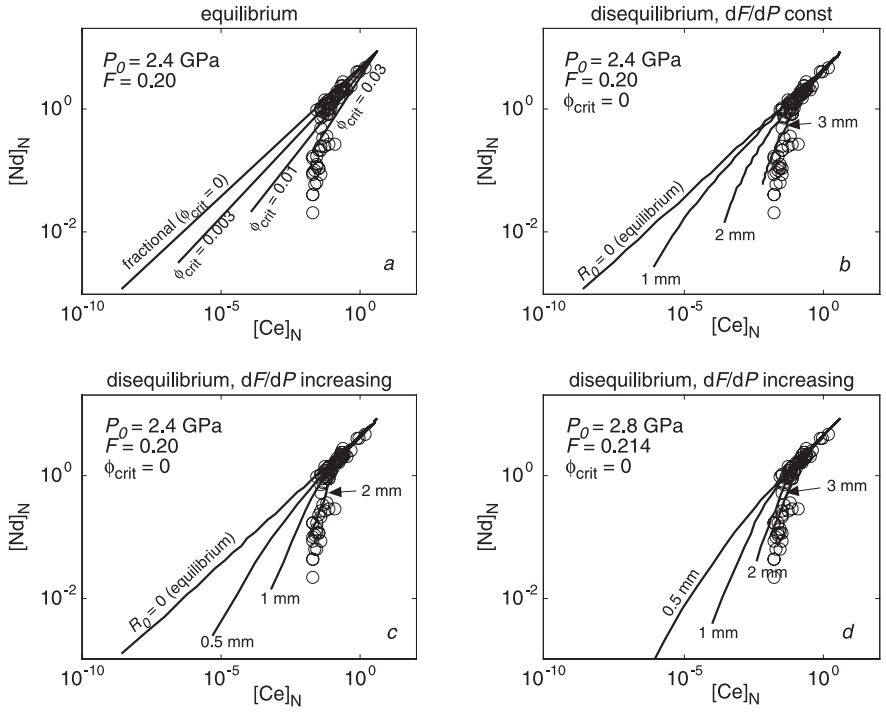

Fig. 8. Comparison of model predictions with observed chondrite-normalized Ce and Nd concentrations in cpx grains from abyssal peridotites (open circles [4,39]). All calculations assume an upwelling rate of 0.9 cm yr^{-1}. (a) Curves show model Ce and Nd concentrations for 0–20% melting in the spinel stability field, with equilibrium maintained between melt and cpx. $P_0 = 2.4$ GPa; $0 < \phi_{crit} < 0.03$. (b) Disequilibrium fractional melting in spinel stability field, with constant melt productivity. $P_0 = 2.4$ GPa; $F = 0.20$; $0 < R_0 < 3$ mm. (c) Disequilibrium fractional melting in spinal stability field, with melt productivity initially constant and increasing linearly with decompression beyond 1.0 GPa. $P_0 = 2.4$ GPa; $F = 0.20$; $0 < R_0 < 2$ mm. (d) Disequilibrium fractional melting beginning in garnet stability field, with the same increasing productivity function as in panel c. $P_0 = 2.8$ GPa; $F = 0.214$; 0.5 mm $< R_0 < 3$ mm.

ence of diffusional zoning profiles in residual cpx would provide clear evidence for disequilibrium melting, and comparison with model profiles would allow quantitative constraints to be placed on the rate and style of melting. Unfortunately, to our knowledge no information yet exists on zoning of REE in cpx grains from abyssal peridotites.

Peter Kelemen (personal communication), using SIMS, has looked for REE zoning profiles in rounded, porphyroclastic opx grains from harzburgite drill cores sampled beneath the East Pacific Rise (EPR) at Hess Deep. No zoning was found for the heavy REE, and light REE concentrations were near detection limits and yielded inconclusive results. If REE diffusion rates in opx are similar to or slower than diffusion rates in cpx, then we would expect heavy REE zoning in these samples given the rapid half-spreading rate of the EPR (6.5 cm yr^{-1} [37]). The absence of zoning could mean that REE diffusion rates are faster in opx than in cpx, although this seems unlikely given that Pb, for example, diffuses an order of magnitude more slowly in opx than in cpx [38]. On the other hand, it may imply that the opx grains have recrystallized, either during or after melting. If opx did indeed recrystallize during melting, this does not necessarily imply the same for cpx, since cpx is considerably more resistant to recrystallization processes than opx (see discussion above).

Although no information exists on REE zoning in residual cpx, we can place some constraints on disequilibrium during melting beneath mid-ocean ridges by examining 'bulk' cpx REE data. Here

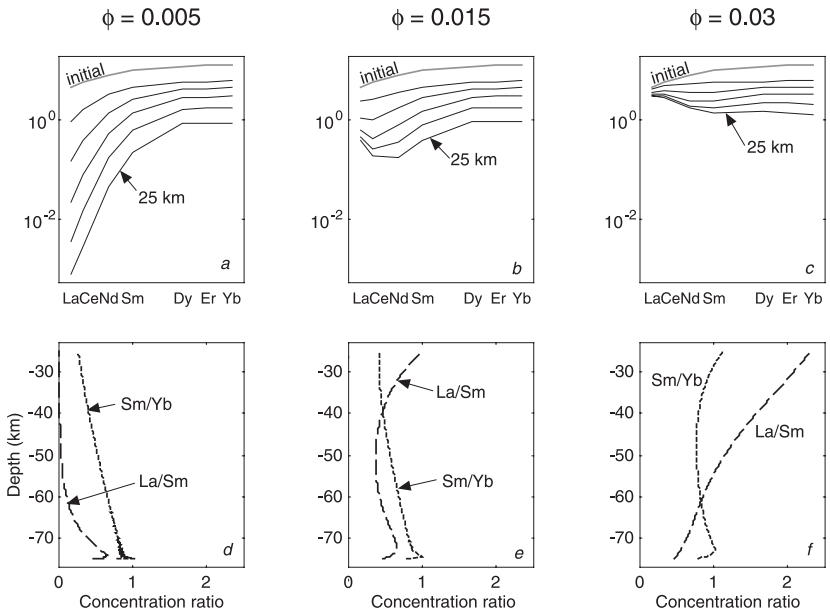

Fig. 9. Predicted evolution of a melt as it ascends through progressively depleted peridotite from 75 to 25 km depth. In panels a–c the gray lines show the initial melt composition and the black lines show melt compositions at 10 km depth intervals. (d–f) [La/Sm] and [Sm/Yb] as continuous functions of depth. (a,d) $\phi = 0.005$, $w = 2.3$ cm yr^{-1}. (b,e): $\phi = 0.015$, $w = 20.6$ cm yr^{-1}. (c,f): $\phi = 0.03$, $w = 82.4$ cm yr^{-1}. In each panel $R = 2$ mm.

we focus on the well-known data sets of Johnson and co-workers [4,39] for cpx grains in abyssal peridotites from the slow-spreading America–Antarctic and Southwest Indian ridge systems. These peridotites are thought to be residues of variable degrees of adiabatic decompression melting with efficient extraction of melt [4]. Fig. 8 shows chondrite-normalized Ce and Nd concentrations in cpx grains, along with model curves representing cpx compositional trajectories during progressive melting under various conditions. Equilibrium models with critical porosity between 0 and 0.03 (Fig. 8a) can account for some of the cpx data, but they do not explain the more depleted compositions and fail to capture the strong concave-downward curvature of the data trend. Models with diffusion-controlled exchange and incomplete equilibration between melt and cpx (Fig. 8b–d) do have concave-downward curvature in Ce vs. Nd, and more closely approximate the observed data trend. The data are best fit by disequilibrium melting models with initial cpx radii of 2–3 mm, which is well within the range of grain sizes observed in peridotite xenoliths.

The concave-downward curvature of the model disequilibrium melting trends results from changes in the partitioning behavior of Ce and Nd during decompression melting. The effective partition coefficients for both elements increase as melting progresses, due to the decrease in temperature. Ce is affected more severely than Nd because of its lower diffusivity, and this is what leads to the concave-downward curvature in the Ce vs. Nd trajectory. Variable productivity models (Fig. 8c,d) have stronger curvature than constant productivity models (Fig. 8b) due to increases in melting rate and degree of disequilibrium as melting proceeds to shallow depths.

4. Diffusive fractionation of REE during melt transport

Above we have considered the influence of diffusion on REE fractionation during adiabatic decompression melting. We have simplified the problem by assuming that the residual melt is in-

stantaneously removed from contact with the solid once the critical melt fraction is exceeded. In reality melts may begin to flow through permeable intergranular networks at very small melt fractions (e.g. [21]), and these small-degree melts may undergo significant diffusive exchange with minerals in the solid matrix. This can result in substantial chemical modification of the melt.

We have used a two-step numerical procedure to investigate the chemical evolution of a melt as it percolates upward through spinel peridotite that has previously been depleted by adiabatic decompression melting. In the mid-ocean ridge setting, the simple two-step process envisioned here may apply most directly to melts that pass upward through depleted lithosphere rather than being focused towards the ridge axis and mixing with shallower melts en route. In the first step, the composition of the solid matrix is calculated as a function of depth using the numerical model described above. Melting is assumed to begin at 2.8 GPa, with 1%melt retained in the solid matrix, an initial grain radius of 2 mm,constant melt productivity of 0.1 GPa^{-1}, and an upwelling rate of 1 cm yr^{-1}. In the second step, residual liquid from some depth in the column moves upward, interacting in turn with solids from successively higher levels. Chemical interaction is assumed to take place via diffusive exchange, with no dissolution or precipitation of solid phases and no changes in melt volume. We have also performed simulations in which the melt dissolves up to four times its mass of cpx as it ascends (e.g. [40]), but this was found to have little influence on the REE composition of the melt because the clinopyroxene is already so depleted, especially at its outer rim.

The melt is assumed to ascend by Darcy flow through a grain-scale porous network within a stationary solid matrix. The melt velocity is given by (e.g. [41]):

$$w = \frac{k\Delta\rho g}{\phi\mu} \tag{13}$$

where k is the permeability, $\Delta\rho$ is the density difference between matrix and melt, g is the acceleration due to gravity and μ is the melt viscosity. The relationship between the permeability k, grain radius R, and porosity ϕ is expressed as:

$$k = \frac{R^2\phi^n}{4b} \tag{14}$$

where n and b are numerical constants. Experi-

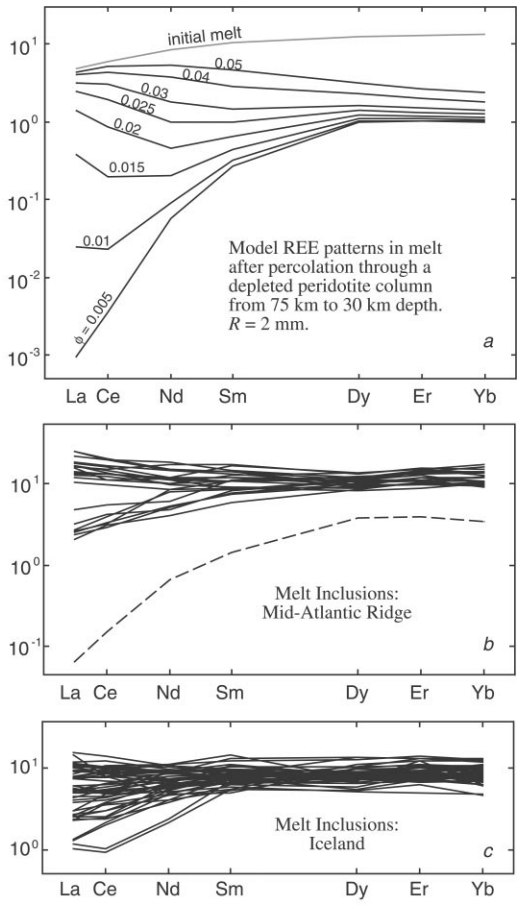

Fig. 10. Comparison of theoretical REE patterns, produced by diffusive fractionation during melt transport, with melt inclusion data. (a) Model REE patterns. The gray line represents the initial melt and the black lines show how it is modified after ascending from 75 to 30 km depth through permeable networks with $R = 2$ mm and porosity between 0.005 and 0.05. The final depth of 30 km corresponds to the depth at which olivine-hosted melt inclusions from the FAMOUS region of the MAR are multiply saturated with a lherzolite residue on their liquidus [26]. (b) Data for olivine-hosted melt inclusions from the MAR. Solid lines [26]; dashed line [45]. (c) Data for olivine-hosted melt inclusions from NE Iceland [44]. Note that all three figures are plotted on the same scale.

mental permeability studies of texturally equilibrated fluid–rock systems with characteristics similar to the olivine–melt system indicate that $n=3$ and $b\approx 270$ [42,43]. The melt velocity is calculated using these values, with $\Delta\rho=500$ kg m^{-3} and $\mu=10$ Pa s. The size and volume fraction of cpx grains decrease upward in the column, but this is not the case for other solid phases and thus R is assumed to be constant when calculating the permeability.

Fig. 9 shows how the REE pattern of the melt evolves as it ascends through the depleted solid column under three different conditions ($\phi=0.005$, $\phi=0.015$ and $\phi=0.03$). When the porosity is very small the melt ascends slowly enough that the melt is able to reequilibrate with the solid matrix. This condition ('equilibrium porous flow') is approached when $\phi=0.005$ (at a melt velocity of 2.3 cm yr^{-1}). Both light and heavy REE are reabsorbed by cpx, and the melt becomes highly depleted (Fig. 9a,d). When the porosity (and melt velocity) are higher (Fig. 9b,c,e,f) the REE are diffusively fractionated. Heavy REE still approach equilibrium with the matrix cpx, but light REE do not and thus the melt develops a pattern of heavy REE depletion (relative light REE enrichment). Melts can avoid any exchange with matrix cpx only if they ascend very rapidly, at a rate greater than $\sim$30 m yr^{-1}. This requires transport in networks with either very high porosity ($\phi>0.2$ for 2 mm grain radii) or with channel spacing significantly greater than the grain size ($\sim$10 cm for $\phi=0.01$).

The effects of diffusive fractionation during melt transport should be most evident in melt inclusions, which, unlike lavas, may be isolated from subsequent chemical modification processes. Olivine-hosted melt inclusions from the Mid-Atlantic Ridge (MAR) [26,45] and from Iceland [44] exhibit a wide variety of REE patterns, many of which are similar to REE patterns predicted to result from diffusive fractionation during melt percolation (Fig. 10). Light REE-enriched patterns are common in melt inclusions from both the MAR and Iceland. These are usually attributed to melting in the presence of garnet, but they could arise in the absence of garnet as a consequence of diffusive exchange with depleted spinel peridotite. Melt inclusions that are extremely depleted in REE (e.g. [45]) may reflect reequilibration with depleted peridotite during sluggish percolation through low-porosity networks. Although it is not possible to identify a unique 'signature' of diffusive fractionation during melt transport, the fact that it can account for much of the chemical variation in melt inclusion suites, at reasonable porosities and grain sizes, suggests that it may be an important melt modification process. It is worth bearing in mind that the REE contents of melts must be modified significantly during transport, unless they are focused at an early stage into a network that has either large channel spacing (with ascent rates >30 m yr^{-1}) or contains no cpx (e.g. dunite channels [46]).

5. Conclusions

We have shown that diffusion may play an important role in trace element fractionation during melting and melt transport beneath mid-ocean ridges. Large, highly charged elements, including the light REE [1], U and Th [13], diffuse so slowly in cpx that complete chemical equilibrium between solid and melt is unlikely to be achieved either during melting or during transport through permeable intergranular networks. Large differences in diffusivity among the REE can lead them to be diffusively fractionated during melting and transport.

The effects of diffusive fractionation during melting are most apparent in the residual solid. Data for the light REE in abyssal peridotite cpx grains from the slow spreading America–Antarctic and Southwest Indian ridge systems are better explained by melting models that allow for diffusive exchange than by models that assume complete solid–melt equilibration. The data are best fit with initial cpx grain radii of $\sim$2–3 mm and very efficient melt extraction (near fractional).

Percolation of small-degree melts through depleted spinel peridotite can lead to significant chemical modification as incompatible elements are diffusively reabsorbed by cpx. Sluggish transport through intergranular networks can lead to very strong depletion in melt REE contents, par-

ticularly if the porosity is very small (<0.005). At moderate porosities (~ 0.02–0.03) the REE are diffusively fractionated and melts may acquire patterns of relative light REE enrichment. Ascending melts can remain chemically isolated from the solid matrix only if they are focused into permeable networks with large channel spacing (ascent rates >30 m yr^{-1}) or which contain no cpx (e.g. dunite channels).

Acknowledgements

We gratefully acknowledge thoughtful reviews by Yan Liang and Daniele Cherniak, and helpful discussions with Peter Kelemen, Ken Koga, Jun Korenaga and Alberto Saal. This work was supported by grants from the National Science Foundation (OCE-9415968 and OCE-9731506) and by an NSF Graduate Research Fellowship.*[AH]*

References

[1] J.A. Van Orman, T.L. Grove, N. Shimizu, Rare earth element diffusion in diopside: influence of temperature, pressure and ionic radius, and an elastic model for diffusion in silicates, Contrib. Mineral. Petrol. 141 (2001) 687–703.

[2] J.A. VanOrman, T.L. Grove, N. Shimizu, G.D. Layne, Rare earth element diffusion in a natural pyrope single crystal at 2.8 GPa, Contrib. Mineral. Petrol. 142 (2002) 416–424.

[3] D. McKenzie, ^{230}Th–^{238}U disequilibrium and the melting process beneath ridge axes, Earth Planet. Sci. Lett. 72 (1985) 149–157.

[4] K.T.M. Johnson, H.J.B. Dick, N. Shimizu, Melting in the oceanic upper mantle: an ion microprobe study of diopsides in abyssal peridotites, J. Geophys. Res. 95 (1990) 2661–2678.

[5] O. Navon, E.M. Stolper, Geochemical consequences of melt percolation: the upper mantle as a chromatographic column, J. Geol. 95 (1987) 285–307.

[6] Z. Qin, Disequilibrium partial melting model and its implications for trace element fractionations during mantle melting, Earth Planet. Sci. Lett. 112 (1992) 75–90.

[7] M. Spiegelman, P. Kenyon, The requirements for chemical disequilibrium during magma migration, Earth Planet. Sci. Lett. 109 (1992) 611–620.

[8] S.R. Hart, Equilibration during mantle melting: a fractal tree model, Proc. Natl. Acad. Sci. USA 90 (1993) 11914–11918.

[9] H. Iwamori, Dynamix disequilibrium melting model with porous flow and diffusion controlled chemical equilibration, Earth Planet. Sci. Lett. 114 (1993) 301–313.

[10] H. Iwamori, A model for disequilibrium mantle melting incorporating melt transport by porous and channel flows, Nature 366 (1993) 734–737.

[11] E.H. Hauri, Melt migration and mantle chromatography, 1: simplified theory and conditions for chemical and isotopic decoupling, Earth Planet. Sci. Lett. 153 (1997) 1–19.

[12] J. Korenaga, P.B. Kelemen, Melt migration through the oceanic lower crust: a constraint from melt percolation modeling with finite solid diffusion, Earth Planet. Sci. Lett. 156 (1998) 1–11.

[13] J.A. Van Orman, T.L. Grove, N. Shimizu, Uranium and thorium diffusion in diopside, Earth Planet. Sci. Lett. 160 (1998) 505–519.

[14] P.D. Asimow, M.M. Hirschmann, E.M. Stolper, An analysis of variations in isentropic melt productivity, Phil. Trans. R. Soc. London A355 (1997) 244–281.

[15] T. LaTourrette, G.J. Wasserburg, A.J. Fahey, Self diffusion of Mg, Ca, Ba, Nd, Yb, Ti, Zr, and U in haplobasaltic melt, Geochim. Cosmochim. Acta 60 (1996) 1329–1340.

[16] S. Karato, P. Wu, Rheology of the upper mantle: a synthesis, Science 260 (1993) 771–778.

[17] S. Karato, Z.C. Wang, B. Liu, K. Fujino, Plastic deformation of garnets: systematics and implications for the rheology of the mantle transition zone, Earth Planet. Sci. Lett. 130 (1995) 13–30.

[18] S.H. Kirby, A.K. Kronenberg, Deformation of clinopyroxenite: evidence for a transition in flow mechanisms and semi-brittle behavior, J. Geophys. Res. 89 (1984) 3177–3192.

[19] S.J. Mackwell, High-temperature rheology of enstatite: implications for creep in the mantle, Geophys. Res. Lett. 18 (1991) 2027–2030.

[20] M. Bystricky, S. Mackwell, Creep of dry clinopyroxene aggregates, J. Geophys. Res. 106 (2001) 13443–13454.

[21] D.L. Kohlstedt, Structure, rheology and permeability of partially molten rocks at low melt fractions, in: J. Phipps Morgan, D.K. Blackman, J. Sinton (Eds.), Mantle Flow and Melt Generation at Mid-Ocean Ridges, American Geophysical Union, Washington, DC, 1992, pp. 103–121.

[22] J.R. Farver, R.A. Yund, D.C. Rubie, Magnesium grain boundary diffusion in forsterite aggregates at 1000–1300°C and 0.1 MPa to 10 GPa, J. Geophys. Res. 99 (1994) 19809–19819.

[23] R.A. Yund, Rates of grain boundary diffusion through enstatite and forsterite reaction rims, Contrib. Mineral. Petrol. 126 (1997) 224–236.

[24] P.B. Kelemen, N. Shimizu, T. Dunn, Relative depletion of niobium in some arc magmas and the continental crust: partitioning of K, Nb, La and Ce during melt/rock reaction in the upper mantle, Earth Planet. Sci. Lett. 120 (1993) 111–134.

[25] V.J.M. Salters, J. Longhi, Trace element partitioning dur-

ing the initial stages of melting beneath mid-ocean ridges, Earth Planet. Sci. Lett. 166 (1999) 15–30.
[26] N. Shimizu, The geochemistry of olivine-hosted melt inclusions in a FAMOUS basalt ALV519-4-1, Phys. Earth Planet. Inter. 107 (1998) 183–201.
[27] R.J. Kinzler, T.L. Grove, Primary magmas of mid-ocean ridge basalts. 2. Applications, J. Geophys. Res. 97 (1992) 6907–6926.
[28] M.J. Walter, Melting of garnet peridotite and the origin of komatiite and depleted lithosphere, J. Petrol. 39 (1998) 29–60.
[29] B.J. Wood, J.D. Blundy, A predictive model for rare earth element partitioning between clinopyroxene and anhydrous silicate melt, Contrib. Mineral. Petrol. 129 (1997) 166–181.
[30] J.D. Blundy, J.A.C. Robinson, B.J. Wood, Heavy REE are compatible in clinopyroxene on the spinel lherzolite solidus, Earth Planet. Sci. Lett. 160 (1998) 493–504.
[31] R.J. Kinzler, T.L. Grove, Primary magmas of mid-ocean ridge basalts. 1. Experiments and methods, J. Geophys. Res. 97 (1992) 6885–6906.
[32] M.B. Baker, E.M. Stolper, Determining the composition of high-pressure mantle melts using diamond aggregates, Geochim. Cosmochim. Acta 58 (1994) 2811–2828.
[33] R.J. Kinzler, Melting of mantle peridotite at pressures approaching the spinel to garnet transition: application to mid-ocean ridge basalt petrogenesis, J. Geophys. Res. 102 (1997) 853–874.
[34] R.J. Kinzler, T.L. Grove, Origin of depleted cratonic harzburgite by deep fractional melt extraction and shallow olivine cumulate infusion, in: J.J. Gurney et al. (Eds.), Proc. 7th Intl. Kimberlite Conf., Red Roof Design, Cape Town, 1999, pp. 437–443.
[35] P.D. Asimow, M.M. Hirschmann, M.S. Ghiorso, M.J. O'Hara, E.M. Stolper, The effect of pressure-induced solid-solid phase transitions on decompression melting of the mantle, Geochim. Cosmochim. Acta 59 (1995) 4489–4506.
[36] K.T. Koga, N. Shimizu, T.L. Grove, Disequilibrium trace element redistribution during garnet to spinel facies transition, in: J.J. Gurney, J.L. Gurney, M.D. Pascoe, S.H. Richardson (Eds.), Proceedings of the 7th International Kimberlite Conference, Vol. 1, Red Roof Design, Cape Town, 1999, pp. 444–451.
[37] P. Lonsdale, Structural pattern of the Galapagos microplate and evolution of the Galapagos triple junctions, J. Geophys. Res. 93 (1988) 13551–13574.
[38] D.J. Cherniak, Pb diffusion in Cr diopside, augite, and enstatite, and consideration of the dependence of cation diffusion in pyroxene on oxygen fugacity, Chem. Geol. 177 (2001) 381–397.
[39] K.T.M. Johnson, H.J.B. Dick, Open system melting and temporal and spatial variation of peridotite and basalt at the Atlantis-II fracture-zone, J. Geophys. Res. 97 (1992) 9219–9241.
[40] P.B. Kelemen, J.A. Whitehead, E. Aharanov, K.A. Jordahl, Experiments on flow focusing in soluble porous media, with applications to melt extraction from the mantle, J. Geophys. Res. 100 (1995) 475–496.
[41] D. McKenzie, Some remarks on the movement of small melt fractions in the mantle, Earth Planet. Sci. Lett. 95 (1989) 53–72.
[42] D.A. Wark, E.B. adn Watson, Grain-scale permeabilities of texturally equilibrated, monomineralic rocks, Earth Planet. Sci. Lett. 164 (1998) 591–605.
[43] Y. Liang, J.D. Price, D.A. Wark, E.B. Watson, Nonlinear pressure diffusion in a porous medium: approximate solutions with applications to permeability measurements using transient pulse decay method, J. Geophys. Res. 106 (2001) 529–535.
[44] L. Slater, D. McKenzie, K. Grönvold, N. Shimizu, Melt generation and movement beneath Theistareykir, NE Iceland, J. Petrol. 42 (2001) 321–354.
[45] A.V. Sobolev, N. Shimizu, Ultra-depleted primary melt included in an olivine from the Mid-Atlantic Ridge, Nature 363 (1993) 151–154.
[46] P.B. Kelemen, G. Hirth, N. Shimizu, M. Spiegelman, H.J.B. Dick, A review of melt migration processes in the adiabatically upwelling mantle beneath ocean spreading ridges, Phil. Trans. R. Soc. London A 355 (1997) 283–318.